

Constraining black hole masses from stellar kinematics by summing over all possible distribution functions

John Magorrian*

Rudolf Peierls Centre for Theoretical Physics, 1 Keble Road, Oxford OX1 3NP

ABSTRACT

When faced with the task of constraining a galaxy’s potential given limited stellar kinematical information, what is the best way of treating the galaxy’s unknown distribution function (DF)? Using the example of estimating black hole (BH) masses, I argue that the correct approach is to consider all possible DFs for each trial potential, marginalizing the DF using an infinitely divisible prior. Alternative approaches, such as the widely used maximum penalized likelihood method, neglect the huge degeneracies inherent in the problem and simply identify a single, special DF for each trial potential.

Using simulated observations of toy galaxies with realistic amounts of noise, I find that this marginalization procedure yields significantly tighter constraints on BH masses than the conventional maximum-likelihood method, although it does pose a computational challenge which might be solved with the development of a suitable algorithm for massively parallel machines. I show that in practice the conventional maximum-likelihood method yields reliable BH masses with well-defined minima in their χ^2 distributions, contrary to claims made by Valluri, Merritt & Emsellem.

Key words: galaxies: nuclei – galaxies: kinematics and dynamics – stellar dynamics – methods: statistical

1 INTRODUCTION

A fundamental application of stellar dynamics is using observations of a galaxy’s kinematics to constrain its potential $\psi(\mathbf{x})$. The galaxy is normally assumed to be collisionless and in a steady state, so that the dynamics of any population of stars are completely described by its phase space distribution function (DF), $f(\mathbf{x}, \mathbf{v})$, which is the probability density of finding a star in the small volume of phase space around (\mathbf{x}, \mathbf{v}) . By Jeans’ theorem, this DF can depend on (\mathbf{x}, \mathbf{v}) only through the integrals of motion of the (unknown) potential.

Most approaches to this task begin by considering the simpler problem of constraining f given the observed data and some trial ψ . The infinite-dimensional DF is parametrized by a finite sum of delta functions (e.g., Schwarzschild 1979) or a truncated basis function expansion (e.g., Dejonghe 1989; Saglia et al. 2000), and the DF parameters are adjusted to optimize the fit to the observations. If no set of parameters yields an acceptable fit while simultaneously representing a DF that is everywhere non negative, then the assumed potential can be ruled out.

This basic idea can be refined further. Richstone & Tremaine (1988) pointed out that naive

application of this method will yield unrealistically spiky DFs, leading them to advocate the use of entropy (or something similar) as a regularizer. This idea of regularizing the resulting DFs was made more explicit by Merritt (1993), who cast the problem as one of finding the maximum penalized log-likelihood, $\mathcal{L}' \equiv -\frac{1}{2}\chi^2 + \lambda P[f]$, which allows a trade off between goodness of fit, as measured by χ^2 , and smoothness, as measured by the penalty function P . The choice of penalty function and the value to use for the tradeoff parameter λ are arbitrary and subjective. Given a range of trial potentials, one finds the maximum penalized likelihood for each and then uses normal statistical methods to make statements about how well constrained the potential is. This general approach has become the method of choice in stellar-dynamical searches for supermassive black holes (hereafter BHs) in galaxy centres, with choices of penalty function ranging from the mean-square second derivative of the DF (e.g., van der Marel et al. 1998; Cappellari et al. 2002) or entropy (e.g., Gebhardt et al. 2003; Silge et al. 2005) through to models in which no regularization whatsoever has been applied (e.g., van der Marel et al. 1998; Houghton et al. 2006). I refer to these as “maximum-likelihood” or “maximum-penalized likelihood” methods.

Another way to look at the problem of constraining potentials is to treat it as a straightforward mathemati-

* E-mail: magog@thphys.ox.ac.uk

cal inverse problem. Dejonghe & Merritt (1992) considered the case of constraining the potential of a spherical galaxy given perfect knowledge of its projected DF in the form of its line-of-sight velocity profiles (hereafter VPs) $L(R; v_p)$. By using a set of higher-order Jeans equations they showed that, given the potential, the DF $f(\mathcal{E}, J^2)$ is completely determined by its projected VPs. Constraining the potential, however, proved less amenable to their methods, but they found that choosing a potential too far from the true one would yield moments (and therefore DFs) that became negative, ruling out that potential.

Of course, one never has perfect knowledge of the full projected DF. More recently, Valluri, Merritt, & Emsellem (2004, hereafter VME04) investigated the slightly less idealized problem of constraining the BH mass in a toy axisymmetric galaxy given noiseless measurements of a restricted number of (modified) moments of its VPs averaged over a number of spatial bins on the sky. They showed that even when the potential has just one free parameter – the BH mass – there are many different potentials that can fit the available kinematics almost perfectly, even when the central spatial resolution of the kinematics is much finer than the BH’s sphere of influence.

One thing that all these methods have in common is that they consider just one DF for each trial potential. This is fine for the idealized case considered by Dejonghe & Merritt (1992): given perfectly resolved, noiseless projected VPs of a spherical galaxy there is a unique DF for any assumed potential, even though this DF may not be non-negative everywhere. But when the available data have finite spatial and velocity resolution, there will in general be many perfectly sensible, non-negative DFs that yield equally good fits to the data, and even more DFs producing fits that are only slightly worse. Intuitively, one might expect that the more such DFs a potential admits, the more likely it is.

The purpose of the present paper is to revisit the the problem of constraining BH masses from a thoroughly Bayesian perspective, showing how it naturally incorporates this intuitive notion of counting up DFs. To illustrate the ideas, I use simulated observations of some idealized spherical toy galaxies described in Section 2, modelling them under the assumptions given in section 3. In section 4 I test how well the conventional maximum likelihood method recovers BH masses and counter some of the more pessimistic conclusions of VME04. Section 5 presents a Bayesian approach to the problem, which overcomes some of the inconsistencies of the maximum likelihood method. Finally, section 6 sums up and discusses the implications for BH masses in real galaxies.

2 TOY GALAXIES

2.1 Intrinsic properties

My toy galaxies are spherical with luminosity density profile (Dehnen 1993; Tremaine et al. 1994)

$$j(r) = \frac{(3-\alpha)L}{4\pi} \frac{a}{r^\alpha(a+r)^{4-\alpha}}, \quad (1)$$

and constant mass-to-light ratio Υ for radii $r > 0$, so that the total stellar mass $M_\star = \Upsilon L$. At $r = 0$ there is a BH of mass $M_\bullet = 2 \times 10^{-3} M_\star$. The galaxies used in this paper all have

inner density slope $\alpha = 1.5$, for which the BH dominates the kinematics inside a radius 0.015a.

By Jeans’ theorem (Binney & Tremaine 1987), a spherical galaxy can be in equilibrium only if its phase-space distribution function (DF) depends on (\mathbf{x}, \mathbf{v}) only through the integrals of motion \mathcal{E} and \mathbf{J} , the energy and angular momentum per unit mass. The DFs of the toy galaxies have the form (Cuddeford 1991)

$$f(\mathcal{E}, J^2) = J^{-2\beta} g(\mathcal{E}), \quad (2)$$

where the parameter β controls the degree of anisotropy, with $\beta = 1 - \sigma_\phi^2/\sigma_r^2$. I solve for $g(\mathcal{E})$ given $j(r)$ and M_\bullet using the method described in Magorrian & Tremaine (1999), and present results for both isotropic ($\beta = 0$) and mildly radially anisotropic ($\beta = 0.3$) toy galaxies.

2.2 Observables

The standard “observations” of each toy galaxy consist of its luminosity-weighted VPs averaged over abutting shells, with 5 shells per decade in radius whose centres run from $R_{\min} = 10^{-3}a$ to $R_{\max} = 4a$. These observations both resolve the BH’s sphere of influence and extend to more than twice the galaxies’ effective radii. I calculate VPs $L(R; v_p)$ using the procedure described in van der Marel et al. (2000) and parametrize each using a Gauss–Hermite series (Gerhard 1993; van der Marel & Franx 1993),

$$L_{\text{GH}}(R; v_p) = \frac{\gamma}{\sqrt{2\pi}\sigma} \exp\left[-\frac{1}{2}\left(\frac{v-V}{\sigma}\right)^2\right] \sum_{i=0}^{\infty} h_i H_i\left(\frac{v-V}{\sigma}\right). \quad (3)$$

This expresses the VP as an underlying Gaussian with normalization γ , mean V and dispersion σ , modified by a sum of Hermite polynomials H_i . For any reasonable choice of (γ, V, σ) it is straightforward to show that choosing

$$h_i = \frac{1}{\sqrt{2\gamma}} \int_{-\infty}^{\infty} \exp\left[-\frac{1}{2}\left(\frac{v-V}{\sigma}\right)^2\right] L(v) H_i\left(\frac{v-V}{\sigma}\right) dv \quad (4)$$

minimizes the mean-square deviation between $L(R; v_p)$ and $L_{\text{GH}}(R; v_p)$. Therefore, the h_i are simply *modified moments* of $L(R; v_p)$. I choose (γ, V, σ) to be the parameters of the best-fitting Gaussian to $L(R; v_p)$, in which case V and the odd h_i are zero, $(h_0, h_2) = (1, 0)$ (by eqs. 3 and 4 above) and h_4 measures the lowest-order departure of the VP from Gaussianity.

Each realization of a toy galaxy then consists of 19 VPs. I expand each VP about its underlying best-fit Gaussian (γ, V, σ) , and reduce the VP to four “measurements”: the mean surface brightness I , and the three lowest-order luminosity-weighted modified moments (Ih_0, Ih_2, Ih_4) . To these I add independent, normally distributed errors $\Delta I = 10^{-3}I$, $(\Delta h_0, \Delta h_2, \Delta h_4) = (0.02, 0.05, 0.05)$, comparable to the formal errors from observations of real galaxies. Notice that the parameters of the underlying Gaussian (γ, V, σ) are *chosen* by me, not measured, and so have no measurement uncertainties.

Some further comments on the use of the modified moments (4) are in order. Houghton et al. (2006) have shown that Gauss–Hermite expansions are not particularly well

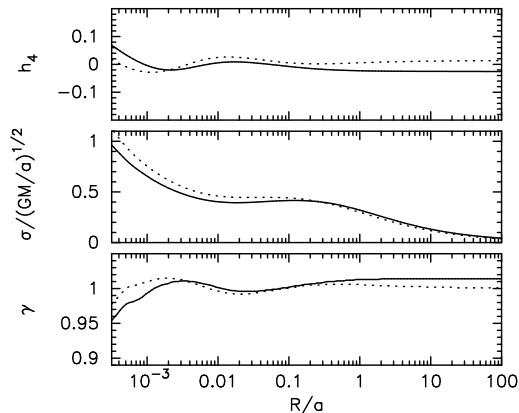


Figure 1. Gauss–Hermite coefficients of the line-of-sight VPs of the isotropic (solid curves) and anisotropic (dotted) toy galaxies.

suit for parametrizing the VPs of real galaxy centres: real VPs can be very strongly non-Gaussian, and in practice measurements of the coefficients h_i are not independent, even for fixed (γ, V, σ) . I nevertheless use the Gauss–Hermite parametrization in the present paper for the following reasons: truncated fourth-order Gauss–Hermite expansions turn out to provide reasonably accurate fits to the VPs of the toy galaxies; real observations have finite velocity resolution, which is mimicked, at least qualitatively, by truncating the infinite Gauss–Hermite expansion (e.g., compare the eigen-VPs in fig. 6 of Houghton et al. (2006) with the Gauss–Hermite basis in fig. 1 of van der Marel & Franx (1993)); finally, using Gauss–Hermite expansions permits a more direct comparison with VME04’s method and results.

3 MODELS

The general modelling scheme is the same as that used in Houghton et al. (2006). The model potentials $\psi(r)$ have two free parameters, the BH mass M_\bullet and the mass-to-light ratio Υ , corresponding to mass densities of the form

$$\rho(r) = \frac{M_\bullet}{4\pi} \delta(r) + \Upsilon j(r), \quad (5)$$

where $j(r)$ is given by (1). Since the kinematics of the toy galaxies are averaged over abutting shells and extend to many effective radii, it turns out that Υ is very well constrained by virtue of the virial theorem (Richstone & Tremaine 1988). So, for the results presented in this paper I simply fix Υ at its correct value. This means that model and galaxy potentials differ only in their BH masses.

Having the potential ψ , I discretize the DF

$$f(\mathcal{E}, J^2) = \sum_{i=1}^{n_\mathcal{E}} \sum_{j=1}^{n_J} f_{ij} \delta(\mathcal{E} - \mathcal{E}_i) \delta(J^2 - J_{ij}^2), \quad (6)$$

on an $n_\mathcal{E} \times n_J$ regular grid in phase space. The points \mathcal{E}_i are chosen through $\mathcal{E}_i = \psi(r_i)$ with the r_i spaced logarithmically between $10^{-5}a$ and 10^3a . There are n_J values of angular momentum for each \mathcal{E}_i , with J_{ij}^2 running linearly between 0 and $J_c^2(\mathcal{E}_i)$, the angular momentum of a circular orbit of

energy \mathcal{E}_i . To avoid a rash of indices I henceforth write the double sum (6) as a single sum over $n \equiv n_\mathcal{E} \times n_J$ points:

$$f(\mathcal{E}, J^2) = \sum_{i=1}^n f_i \delta(\mathcal{E} - \mathcal{E}_i) \delta(J^2 - J_i^2). \quad (7)$$

This discretization effectively partitions phase space into abutting rectangular cells, with the luminosity contained in each cell being given by

$$L_i \equiv f_i \int_{V_i} g(\mathcal{E}, J^2) d\mathcal{E} dJ^2, \quad (8)$$

where $g(\mathcal{E}, J^2)$ is the density of states for the potential ψ and V_i the volume occupied by the cell. In section 5.1 it will provide convenient to use a dimensionless luminosity

$$F_i \equiv \frac{L_i}{L_s}, \quad (9)$$

where L_s is a characteristic luminosity scale.

The models’ projected observables $I(R)$, $Ih_i(R)$ depend linearly on the orbit weights f_i , so that the χ^2 of a model with DF $\mathbf{f} \equiv (f_1, \dots, f_n)^T$ is the quadratic form

$$\chi^2(\mathbf{f}|\psi) = [\mathbf{Q} - P(\psi) \cdot \mathbf{f}]^T \cdot [\mathbf{Q} - P(\psi) \cdot \mathbf{f}], \quad (10)$$

where

$$\mathbf{Q} \equiv \left(\frac{I(R_1)}{\Delta I(R_1)}, \frac{Ih_0(R_1)}{\Delta Ih_0(R_1)}, \dots, \frac{Ih_4(R_N)}{\Delta Ih_4(R_N)} \right)^T \quad (11)$$

is a column vector containing the list of observations, normalized by their uncertainties, and $P(\psi)$ is a projection matrix whose n columns contain the contribution each DF component makes to the model’s prediction for \mathbf{Q} . The calculation of $P(\psi)$ is described in Appendix A.

4 FITTING MODELS TO OBSERVATIONS: THE MAXIMUM-LIKELIHOOD METHOD

Having a set of observations of a toy galaxy, let us first test how well a simplified version of the standard maximum-likelihood method (e.g., van der Marel et al. 1998; Gebhardt et al. 2003; Valluri, Merritt, & Emsellem 2004; Houghton et al. 2006) reproduces the correct BH mass and its uncertainties. The procedure is as follows:

- (i) choose a trial BH mass M_\bullet and calculate the corresponding potential ψ ;
- (ii) calculate the projection matrices $P(\psi)$ appearing in (10);
- (iii) use a non-negative least-squares algorithm (Lawson & Hanson 1974) to find $\chi_{\min}^2(\psi)$, the minimum value of (10) subject to the constraint that all $f_i \geq 0$;
- (iv) assign a likelihood $\exp[-\frac{1}{2}\chi_{\min}^2(\psi)]$ to the potential ψ .

One obtains constraints on M_\bullet by considering a range of M_\bullet and comparing their relative likelihoods. To keep the interpretation of the results as simple as possible, I do not impose any regularization on the f_i . Section 4.3 below discusses this further.

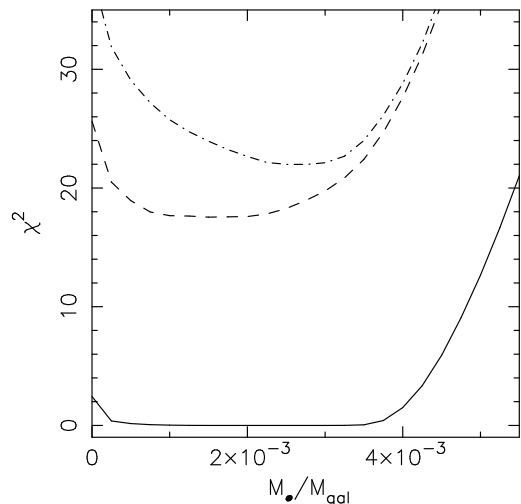


Figure 2. χ^2 distributions returned by the conventional maximum-likelihood method (section 4) for noiseless observations of an isotropic toy galaxy (solid curve) and for two different realizations of observations with simulated noise (dashed and dot-dashed curves).

4.1 VME04’s flat-bottomed $\chi^2(M_\bullet)$ distributions

One of the more alarming conclusions reached by VME04 was that the problem of constraining BH masses is inherently strongly degenerate; they found that a wide range of BH masses could provide equally good fits to mock kinematics with realistic spatial resolution. The main goal of this section of the present paper is to understand this result and to investigate whether its implications really are as negative as VME04 suggest.

The solid curve in figure 2 plots $\chi^2(M_\bullet)$ obtained for models with $n_\varepsilon \times n_J = 100 \times 10$ DF components when applied to noise-free observations of the isotropic toy galaxy. It demonstrates that VME04’s central result also holds for the simpler spherical case considered here: a wide range of M_\bullet can produce perfect fits to perfect noiseless data. For BH masses in the range $1.8 \times 10^{-3} \lesssim M_\bullet/M_{\text{gal}} \lesssim 3.0 \times 10^{-3}$, χ^2 is of order 10^{-25} , rising to $\sim 10^{-5}$ for $M_\bullet/M_{\text{gal}} = 1.7 \times 10^{-3}$ or 3.1×10^{-3} . A model with *no* BH can produce kinematics that differ by only a small amount ($\Delta\chi^2 = 2.4$) from the toy galaxy’s. Of course, these values of χ^2 are statistically meaningless since they do not account for the fact that the observations in this contrived situation have zero uncertainty; the increase of χ^2 to 10^{-5} from its minimum value of 10^{-25} (which is zero to machine precision) is actually very significant.

The other two curves in figure 2 show the results of adding two different realizations of noise to the simulated dataset. This makes $\chi^2(M_\bullet)$ become nicely rounded, similar to what one finds in models of real galaxies (e.g., van der Marel et al. 1998; Gebhardt et al. 2003). VME04, however, only presented results for the noiseless case.

These results can be explained by remembering that, for a fixed potential, χ^2 is a quadratic form (10) in the orbit weights \mathbf{f} . Since the number of unknowns is very much less than the number of observations, this quadratic form is hugely degenerate: it resembles more a multi-dimensional trough than a parabola. If we relax the constraint that all

$f_i \geq 0$, then it turns out that for all the models considered here – independent of the value of M_\bullet – the value of χ^2 at the bottom of the trough is zero (to machine precision); the non-negativity constraint is essential for constraining the BH mass. Of course, for the correct model with $M_\bullet = 2 \times 10^{-3}$, the bottom of the trough passes through the discretized version of the true DF (2), which is well away from the boundaries given by $f_i \geq 0$. Then making a small change in the trial M_\bullet leads to a small change in the projection matrix, particularly for those f_i corresponding to the most tightly bound orbits, and therefore changes the shape of the quadratic form slightly as well as the location of its minimum. Changing the potential too much moves the location of the minimum to a region where at least one of the weights becomes negative, so that the minimum value of χ^2 in the subvolume $f_i \geq 0$ is no longer zero.

Adding noise simply shifts the centre of the quadratic form, with no change in its shape. For realistic amounts of noise, the centre is shifted well into the region where many of the orbit weights are negative, leading to the rounded $\chi^2(M_\bullet)$ profiles.

4.2 The effects of signal to noise on the uncertainties on M_\bullet

In order to examine this more quantitatively, let us consider how the uncertainties on M_\bullet depend on the signal-to-noise ratio of the simulated data. To do this, we need a method of quantifying the uncertainty on M_\bullet . The accepted practice in this field is to assume that the $\Delta\chi^2 = 1$ boundaries of $\chi^2_{\text{min}}(M_\bullet)$ give reliable indicators of the 68 percent confidence limits on M_\bullet (e.g., van der Marel et al. 1998). This is based on the assumption (e.g., Press et al. 1992) that $\chi^2_{\text{min}}(M_\bullet)$ is close to quadratic and therefore that the probability distribution $\exp(-\chi^2_{\text{min}}/2)$ is almost Gaussian, but the results above and in VME04 show that this assumption can be far from the truth. So, throughout this paper I use the mean and variance,

$$\begin{aligned} \overline{M_\bullet} &\equiv A \int M_\bullet \exp\left[-\frac{1}{2}\chi^2_{\text{min}}(M_\bullet)\right] dM_\bullet, \\ (\Delta M_\bullet)^2 &\equiv A \int (M_\bullet - \overline{M_\bullet})^2 \exp\left[-\frac{1}{2}\chi^2_{\text{min}}(M_\bullet)\right] dM_\bullet, \end{aligned} \quad (12)$$

to quantify the best-fitting M_\bullet and its associated uncertainty, the quantity A being chosen to make $A \int \exp[-\chi^2_{\text{min}}] dM_\bullet = 1$. I find that this ΔM_\bullet agrees well with the (correctly calculated) 68 percent confidence intervals for the following.

Figure 3 shows how $\overline{M_\bullet}$ and ΔM_\bullet vary as one changes the size of the observational uncertainties for one particular noise realization $\Delta\mathbf{Q}$, the errors $(\Delta I/I, \Delta h_0, \Delta h_2, \Delta h_4) = s\Delta\mathbf{Q}$ being shrunk by a factor s with respect to the “standard” observational errors. The following points hold for typical noise realizations $\Delta\mathbf{Q}$:

- (i) Given noiseless data ($s = 0$), a range of M_\bullet spanning $1.2 \times 10^{-3} M_{\text{gal}}$ can produce perfect fits. This is essentially the “ $\Delta\chi^2 = 1$ ” measure of the uncertainty on M_\bullet applied to a uniform distribution.
- (ii) The variance of a distribution uniform for $x \in [a, b]$ is given by $(b - a)^2/12$. Therefore, the more useful estimate of

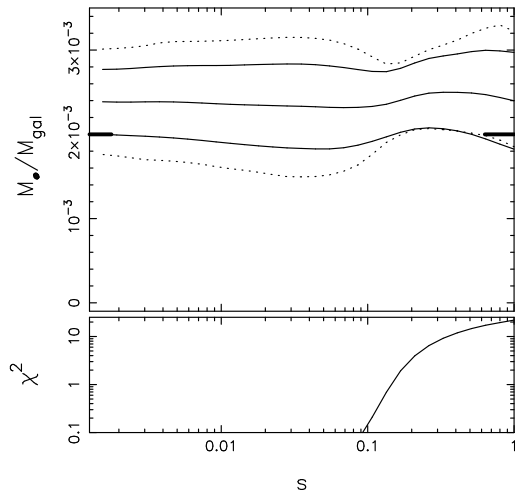


Figure 3. Effect of relative signal-to-noise ratio, $1/s$, on the BH mass M_\bullet returned by the maximum-likelihood method for a typical realization of the noise in the observations. The solid curves in the top panel plots the mean M_\bullet and its formal uncertainty (eq. 12) as a function of s , the relative size of the observational errors. For comparison, the dotted curves show the uncertainties on M_\bullet returned by the widely used $\Delta\chi^2 = 1$ criterion. The bottom panel plots the corresponding minimum value of χ^2 . The $s = 1$ case corresponds to the dot-dashed curve in figure 2.

Table 1. BH mass estimates for toy galaxies using the conventional maximum-likelihood method

β	$n_E \times n_J$	R_{\min}/a	$\langle M_\bullet/10^{-3}M_{\text{gal}} \rangle$	$\langle \Delta(M_\bullet/10^{-3}M_{\text{gal}})^2 \rangle^{1/2}$
0	100×10	10^{-3}	2.08	0.81
0	200×20	10^{-3}	2.10	0.85
0	100×10	10^{-4}	1.89	0.34
0.3	100×10	10^{-3}	2.57	0.99
0.3	200×20	10^{-3}	2.55	1.06
0.3	100×10	10^{-4}	2.08	0.42

Columns are: the galaxy’s anisotropy (β), the number of orbits used in the modelling ($n_E \times n_J$) and the innermost extent of the projected kinematics (R_{\min}); the mean BH mass from many realizations ($\langle M_\bullet \rangle$) and the typical formal uncertainty in M_\bullet .

the uncertainty given by equ. (12) is a factor $\sqrt{12}$ smaller, or $0.35 \times 10^{-3} M_{\text{gal}}$.

(iii) One can obtain perfect fits to the data for any $s \lesssim 0.1$, the precise upper bound on s depending on the particular noise realization.

(iv) Around the value of s where the best-fitting χ^2 starts to lift off from zero, the uncertainty ΔM_\bullet drops as s increases.

(v) Overall, ΔM_\bullet grows slowly with s ; it grows by only a factor ~ 1.5 between the noise-free $s = 0$ and the more realistic $s = 1$ situation.

At first sight the last point might seem to suggest that there is little point in obtaining very high signal-to-noise observations, but of course one could extract higher-order information on the VPs from such observations, such as h_6 or its equivalent, and, in some cases, one could also use finer spatial binning. Both of these would act to reduce the degeneracy in M_\bullet for $s = 0$.

Having examined the effects of observational uncertainties on the uncertainty on M_\bullet , let us now turn to the simpler question of whether the maximum-likelihood method yields estimates of M_\bullet close to the true BH mass. Taking the $s = 1$ situation of realistic noise and averaging over many hypothetical datasets, the typical formal error in M_\bullet is about $0.8 \times 10^{-3} M_{\text{gal}}$ (isotropic galaxy) or $1 \times 10^{-3} M_{\text{gal}}$ (anisotropic galaxy), both increasing only slightly as the number of DF components used increases (Table 1). The maximum-likelihood method yields fairly strongly biased estimates of M_\bullet for the anisotropic galaxy, which nevertheless are well within the formal uncertainties.

4.3 The appropriateness of regularization

Apart from the strange dependence of the formal uncertainty ΔM_\bullet on the signal-to-noise ratio, perhaps the most telling feature of models obtained using the maximum-likelihood method is how well they fit: they are too good to be true. While adding realistic amounts of noise to the observations removes the flat bottom in χ^2 , the value of χ^2 at the minimum remains very much less than the number (76) of observed data points (e.g., figure 2). These fits are implausibly good; the chances are tiny that the actual values of (I, h_0, h_2, h_4) in the real galaxy are all so close to the observed estimates. Furthermore, the models achieve this level of fit by having only ~ 70 of the f_i greater than zero: the internal kinematics of the model are very irregular. It is important then to consider how M_\bullet is affected when one includes models that yield more plausible fits to the data.

Following Merritt (1993), the approach advocated by VME04 and subsequently by Cretton & Emsellem (2004) is to regularize the DF, finding for each M_\bullet the $\{f_i\}$ that maximize a penalized log-likelihood, $-\frac{1}{2}\chi^2 + \lambda P[f]$. The penalty function $P[f]$ provides some arbitrary measure of the smoothness of the DF and the parameter λ is set by how much one is willing to trade off goodness-of-fit for a smoother DF. Although beguiling, this approach is only marginally better than the conventional maximal likelihood method used above, because both

- (i) identify a single privileged “best” DF;
- (ii) and then take this DF to be representative of *all* of the DFs for the assumed potential.

The first step is fine (at least for certain applications), but the second is wholly unjustified and ignores the fact that $\chi^2[f]$ is hugely degenerate.

To see a variant of this problem in a much milder context, consider how one measures M_\bullet in real galaxies. The potential then has at least one additional free parameter, the mass-to-light ratio Υ , and one has to construct a grid of models for a range of different values of M_\bullet and Υ . The uncertainties on M_\bullet are never obtained by picking out a special value of Υ for each M_\bullet ; instead one marginalizes Υ either explicitly (e.g., Gebhardt et al. 2003) or implicitly through the use of a $\Delta\chi^2$ criterion (e.g., van der Marel et al. 1998; Cappellari et al. 2002). This idea of marginalization is key to resolving the issues noted above.

5 FITTING MODELS TO OBSERVATIONS: A BAYESIAN APPROACH

The maximum-likelihood approach of the previous section pays scant attention to the orbit weights f_i , which serve merely as co-ordinates used to locate a point somewhere along the degenerate minimum in χ^2 . From a Bayesian point of view, however, the f_i are *nuisance parameters*. Although we are not interested knowing their precise values, they deserve to be treated on an equal footing with the parameters defining the potential.

Applying Bayes' theorem twice, the posterior probability of a model with potential ψ and a set of orbit weights \mathbf{f} ,

$$p(\psi, \mathbf{f}|D) \propto p(D|\mathbf{f}, \psi)p(\mathbf{f}|\psi)p(\psi), \quad (13)$$

where $p(D|\psi, \mathbf{f}) = \exp[-\frac{1}{2}\chi^2(\mathbf{f}|\psi)]$ is the usual likelihood and the priors $p(\mathbf{f}|\psi)$ and $p(\psi)$ will be discussed later. Since we are not interested in the values of weights (as long as they are non-negative), let us marginalize (13) to obtain

$$p(\psi|D) \propto p(D|\psi)p(\psi), \quad (14)$$

where the marginalized likelihood,

$$\begin{aligned} p(D|\psi) &\equiv \int p(D|\mathbf{f}, \psi)p(\mathbf{f}|\psi) d\mathbf{f} \\ &\equiv \exp\left[-\frac{1}{2}\chi_{\text{marg}}^2\right], \end{aligned} \quad (15)$$

is obtained by summing the likelihood over all non-negative DFs, each weighted by the as-yet-unspecified prior $p(\mathbf{f}|\psi)$. Notice that this is directly analogous to the partition function in statistical mechanics, with χ^2 playing the role of energy and the prior standing in for the density of states. The conventional maximum-likelihood method of the last section can be viewed as the very crude approximation

$$p(D|\psi) \sim \max_{\{\mathbf{f}\} \geq 0} p(D|\mathbf{f}, \psi) = \exp\left[-\frac{1}{2} \min_{\mathbf{f} \geq 0} \chi^2[\mathbf{f}]\right], \quad (16)$$

obtained by completely ignoring the prior $p(\mathbf{f}|\psi)$ and approximating the remaining integral by the peak value of its integrand. There is a straightforward and obvious analogue for the maximum penalized likelihood method.

5.1 The priors

There is nothing noteworthy about the choice of the potential prior $p(\psi)$ for the situation considered here. The potential has one free parameter, M_\bullet , which can be zero or positive, meaning that the natural prior to use is flat in $\log M_\bullet$.

The choice of prior for the DF, $p(\mathbf{f}|\psi)$, is more interesting. Recall that we use discrete cells (7) to model continuous phase space. Now, there is no a priori natural way to partition phase space into cells. Let us assume for the moment that there are no correlations among cells and that the prior is independent of location in phase space. Let μ_i be the prior expectation value for the dimensionless luminosity $F_i \equiv L_i/L_s$ (eq. 9) in cell i ; it can therefore be thought of as measure of the cell's volume. Then a natural requirement on the prior is that, given a partition π of phase space, we should be able to select any cell and construct a new partition π' by subdividing this cell into $m > 0$ subcells and have

that

$$\begin{aligned} p_\pi(F|\mu, \psi) &= \int_0^F dF_1 \cdots \int_0^F dF_m \delta(F_1 + \cdots + F_m - F) \\ &\quad \times p_{\pi'}(F_1|\mu_1, \psi) \times \cdots \times p_{\pi'}(F_m|\mu_m, \psi), \end{aligned} \quad (17)$$

where the cell volumes satisfy $\mu_1 + \cdots + \mu_m = \mu$. That is, marginalizing over the subcells should return the original prior. A consequence of this is that, for finite-resolution data, the marginalized likelihood $p(D|\psi)$ is independent of the chosen partition provided only that one uses fine enough cells.

The infinite-divisibility (hereafter ID) condition (17) puts strong constraints on the form of the prior. It is not satisfied by any of the simplest commonly used priors

$$p(F|\psi) \propto \begin{cases} 1, & \text{(uniform)} \\ 1/F, & \text{(Jeffreys),} \\ \exp[-\alpha F \ln F] & \text{(entropy).} \end{cases} \quad (18)$$

The form of the convolution in eq. (17) suggests that Laplace transforms might be helpful in finding ID priors, and indeed it can be shown (Feller 1971, §XIII.7) that a probability distribution $p(F|\mu)$ satisfies (17) if and only if its Laplace transform

$$\tilde{p}(s|\mu) \equiv \int_0^\infty dF e^{-sF} p(F|\mu) \quad (19)$$

is of the form

$$\tilde{p}(s|\mu) = \exp\left[-\int_0^\infty \frac{1 - e^{-sF}}{F} \mathcal{M}(\mu, dF)\right], \quad (20)$$

with the only constraint on the measure $\mathcal{M}(\mu, dF)$, known as the *Lévy measure*, being that the integral

$$\int_\epsilon^\infty F^{-1} \mathcal{M}(\mu, dF) \quad (21)$$

converges for all $\epsilon > 0$. Thus we can construct priors that are guaranteed to be ID simply by considering a variety of choices for \mathcal{M} . For example, substituting $\mathcal{M}(\mu, dF) = \mu\delta(F-1) dF$ in (20) results in the Poisson distribution, while $\mathcal{M}(\mu, dF) = \mu e^{-F} dF$ gives the gamma distribution. Both of these obviously satisfy the ID criterion (17).

A concise and very readable introduction to this subject is given by Skilling (1998). He argues that the maximally ignorant choice of \mathcal{M} when one knows only a characteristic scale for F is

$$\mathcal{M}(\mu, dF) = \mu F e^{-F} dF. \quad (22)$$

This results in the so-called ‘‘massive inference’’ prior

$$\begin{aligned} p(F_i|\mu_i, \psi) &= e^{-\mu_i} \left[\delta(F_i) \right. \\ &\quad \left. + \exp(-F_i) \sqrt{\frac{\mu_i}{F_i}} I_1\left(2\sqrt{\mu_i F_i}\right) \right], \end{aligned} \quad (23)$$

where I_1 is the first-order modified Bessel function of the first kind. Appendix B gives an elementary derivation of this prior, explaining how it is the natural generalization of entropy to continuous distributions. I adopt it for the calculations below.

There remains the question of what to choose for the

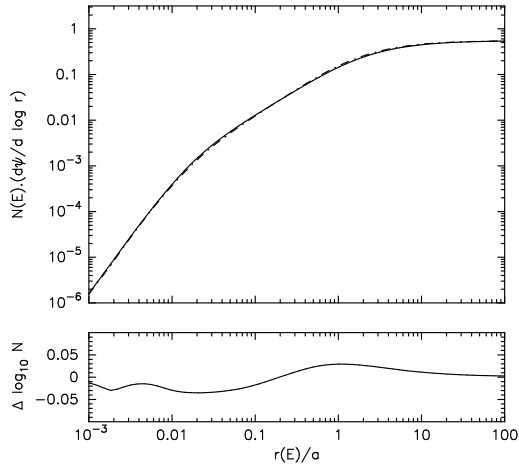


Figure 4. The differential energy distribution $N(\mathcal{E})$ (equ. 25) for isotropic (solid curve) and anisotropic (dashed) toy galaxies, along with their difference (bottom panel). $r(\mathcal{E})$ is the apocentre radius of a perfectly radial orbit with energy \mathcal{E} .

prior weights μ_i . From the Laplace transform (20) it is straightforward to show that the prior mean and variance,

$$\begin{aligned} E(F) &= \int_0^\infty \mathcal{M}(\mu, dF), \\ \text{var}(F) &= \int_0^\infty F \mathcal{M}(\mu, dF), \end{aligned} \quad (24)$$

and therefore that the prior (23) likes to have $F \approx \mu \pm \sqrt{2\mu}$. In the absence of a compelling model of galaxy formation, I simply use the well-known fact (Binney & Tremaine 1987) that for reasonable galaxy models the differential energy distribution,

$$N(\mathcal{E}) = \int_0^{J^2_{\max}(\mathcal{E})} f(\mathcal{E}, J^2) g(\mathcal{E}, J^2) dJ^2, \quad (25)$$

is almost independent of anisotropy once the galaxy's luminosity density $j(r)$ and potential $\psi(r)$ have been specified (e.g., see fig. 4). For each trial potential I find the isotropic DF $f_{\text{iso}}(\mathcal{E})$ that produces the luminosity density (1) and, following (8) and (9), assign

$$\mu_i = \frac{1}{L_s} \cdot \int_{V_i} f_{\text{iso}}(\mathcal{E}) g(\mathcal{E}, J^2) d\mathcal{E} dJ^2. \quad (26)$$

This depends on the choice of characteristic luminosity scale L_s (equ. 9). Now, the prior RMS fractional spread in each cell is equal to $\sqrt{2/\mu_i}$, which clearly depends on L_s and has a Poisson-like $N^{-1/2}$ dependence on the cell volume.¹ In order to make the prior variance independent of the partitioning scheme used to represent the DF, I introduce a second, independent reference partition and choose

$$L_s(\mathcal{E}, J^2) = \frac{2}{\delta^2} \int_{V_{\text{ref}}(\mathcal{E}, J^2)} f_{\text{iso}}(\mathcal{E}) g(\mathcal{E}, J^2) d\mathcal{E} dJ^2, \quad (27)$$

so that the prior RMS fractional spread in each reference cell is given by the adjustable parameter δ . For the results

¹ This is inevitable for any ID distribution, which can be seen either from (24) or from the fact that any ID prior is a limit of a sequence of compound Poisson distributions (Feller 1971).

presented here I use the partition defined by the $n_{\mathcal{E}} \times n_J = 100 \times 10$ grid for this reference partition.

5.2 Marginalization

Although one could attempt the difficult task of evaluating the marginalized likelihood $p(D|\psi)$ (eq. 15) directly, we are not so much interested in the absolute value of $p(D|\psi)$ as in the odds,

$$\frac{p(\psi_1|D)}{p(\psi_0|D)} = \frac{p(D|\psi_1)p(\psi_1)}{p(D|\psi_0)p(\psi_0)}, \quad (28)$$

of one potential ψ_1 compared to another ψ_0 . I evaluate the ratio $p(D|\psi_1)/p(D|\psi_0)$ using the method of thermodynamic integration (Neal 1993). Consider two models, one having potential ψ_0 , the other with a slightly different potential ψ_1 , but both having $n_{\mathcal{E}} \times n_J$ DF components chosen according to the scheme described in section 3 for their respective potentials. Let

$$Z_\lambda \equiv \int \exp[C_\lambda(\mathbf{f})] d\mathbf{f} \quad (29)$$

where

$$\begin{aligned} C_\lambda(\mathbf{f}) &\equiv -\frac{1}{2} [(1-\lambda)\chi^2(\mathbf{f}|\psi_0) + \lambda\chi^2(\mathbf{f}|\psi_1)] \\ &\quad + (1-\lambda) \ln p(\mathbf{f}|\psi_0) + \lambda \ln p(\mathbf{f}|\psi_1). \end{aligned} \quad (30)$$

As the parameter λ varies between 0 and 1, Z_λ interpolates smoothly between $p(D|\psi_0)$ and $p(D|\psi_1)$. Taking the logarithm of (29) and differentiating with respect to λ ,

$$\begin{aligned} \frac{d}{d\lambda} \log Z_\lambda &= \int \frac{dC_\lambda}{d\lambda} \cdot \frac{1}{Z_\lambda} \exp[C_\lambda(\mathbf{f})] d\mathbf{f} \\ &= \left\langle \frac{dC_\lambda}{d\lambda} \right\rangle_\lambda, \end{aligned} \quad (31)$$

where $\langle C \rangle_\lambda$ denotes the expectation value of $C(\mathbf{f})$ when \mathbf{f} has probability density $\exp[C_\lambda(\mathbf{f})]/Z_\lambda$. Therefore we can use a Markov-Chain Monte Carlo method to draw points from this density, and taking the mean value of $dC_\lambda/d\lambda$ for these points gives an immediate estimate of $d \log Z_\lambda / d\lambda$. Then, integrating,

$$\begin{aligned} \int_0^1 d\lambda \cdot \left(\frac{d}{d\lambda} \log Z_\lambda \right) &= \log \left(\frac{Z_1}{Z_0} \right) = \log \left(\frac{p(D|\psi_1)}{p(D|\psi_0)} \right) \\ &= -\frac{1}{2} (\chi_{\text{marg}}^2(\psi_1) - \chi_{\text{marg}}^2(\psi_0)). \end{aligned} \quad (32)$$

This method will be reasonably efficient only if the dependence of $C_\lambda(\mathbf{f})$ on \mathbf{f} does not vary significantly as λ changes, which is the case for the choice of f_i using the scheme described in Section 3.

For the results presented below I use a Gibbs sampler to draw 5×10^6 points from $\exp[C_\lambda(\mathbf{f})]$ after a burn-in period of 10^6 iterations starting from $\mathbf{F} = \boldsymbol{\mu}$. Instead of evaluating the derivative (31) for a range of fixed λ I instead increase λ slowly from 0 to 1 over the course the iterations, yielding $\log p(D|\psi_1) - \log p(D|\psi_0)$ directly. A direct test of this procedure is to run it backwards by swapping the potentials around and calculating $\log p(D|\psi_0) - \log p(D|\psi_1)$. I find that that both forward and backward iterations typically agree very well, provided $\delta \lesssim 20$. For larger δ , the delta function in the prior (23) becomes dominant and the posterior becomes effectively stuck at $F_i = 0$ for a significant fraction of the DF components.

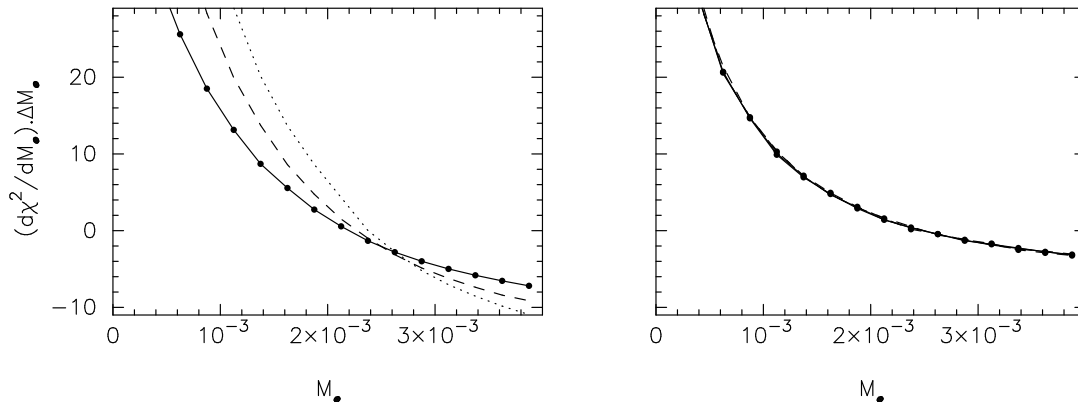


Figure 5. The importance of infinite divisibility. The left panel plots the derivatives of the marginalized log-likelihood $\chi_{\text{marg}}^2(M_\bullet) = -2 \ln p(D|M_\bullet)$ calculated using equ. (32) for a non-ID flat prior. Solid, dashed and dotted curves correspond to models with $n_\mathcal{E} \times n_J = 100 \times 10$, 200×10 and 200×20 DF components, respectively. The panel on the right plots the same for the ID prior (23) with $\delta = 5$.

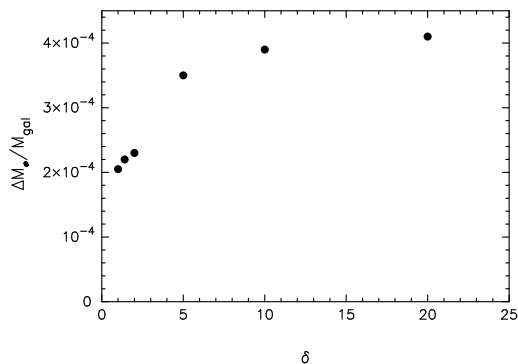


Figure 6. The dependence of the formal uncertainty in BH mass on the fractional variance δ^2 used in the prior.

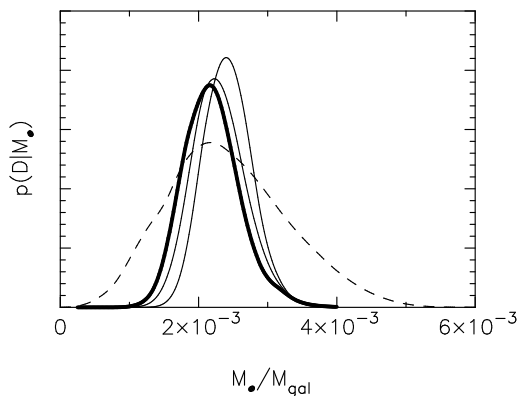


Figure 7. Marginalized likelihoods for one realization of the anisotropic toy galaxy. The solid curves plot $p(D|M_\bullet)$ using priors with $\delta = 5, 10$ and (heavy solid curve) 20 . For comparison, the dashed curve plots the corresponding probability distribution returned by the conventional maximum-likelihood method.

5.3 Results

Here I present results of applying the Bayesian analysis to observations of the anisotropic toy galaxy. The results for

the isotropic galaxy are similar but less instructive since I use the isotropic case to assign the prior weights μ .

Figure 5 demonstrates the importance of using a prior that satisfies the ID criterion (17). Taking a (non-ID) prior flat in the orbit weights \mathbf{f} leads to a marginalized likelihood $p(D|\psi)$ that depends on the number of orbits used and, more generally, on exactly how one discretizes phase space. In contrast, the marginalized likelihood $p(D|M_\bullet)$ for the ID prior (23) does not depend on whether we discretize using $n_\mathcal{E} \times n_J = 100 \times 10$, 200×10 or 200×20 cells. Incidentally, this also shows that, for the present purposes at least, it is acceptable to use delta functions (eq. 7) to calculate the contribution each cell makes to the observations.

Although the marginalized likelihood is independent of the discretization, it still has one free parameter, the fractional variance per reference cell δ^2 . To investigate the dependence of the results on δ , I use the mean and variance of the posterior distribution $p(M_\bullet|D, \delta)$,

$$\begin{aligned} \overline{M_\bullet}(\delta) &= \int M_\bullet p(D|M_\bullet, \delta) p(M_\bullet) dM_\bullet \\ (\Delta M_\bullet(\delta))^2 &= \int (M_\bullet - \overline{M_\bullet}(\delta))^2 p(D|M_\bullet, \delta) p(M_\bullet) dM_\bullet. \end{aligned} \quad (33)$$

Figure 6 shows how the formal uncertainty ΔM_\bullet varies with δ for a typical realization of the observations. As one might expect, ΔM_\bullet is low for small $\delta \sim 1$, but grows rapidly as δ increases. Once δ reaches ~ 10 though, ΔM_\bullet stabilizes at about $0.4 \times 10^{-3} M_{\text{gal}}$. The marginalized likelihoods $p(D|M_\bullet)$ used in calculating ΔM_\bullet for the three largest values of δ plotted are shown in Figure 7, which shows that there is little change as one increases δ from 10 to 20. It is somewhat surprising that δ needs to be so large. This might be a consequence of the power-law dependence of the DF (eq. 2) on J . For comparison, the figure also includes the probability distribution returned by applying the conventional maximum-likelihood method to the same dataset. Taking many realizations of the galaxy, the Bayesian method yields a mean ΔM_\bullet of $0.44 \times 10^{-3} M_{\text{gal}}$ compared to the $0.99 \times 10^{-3} M_{\text{gal}}$ returned by the conventional method (table 1).

6 CONCLUSIONS

Most BH mass estimates come from the conventional maximum-likelihood method. They fit observations using models with specially constructed, unrealistically spiky DFs, yielding implausibly good fits to the observations. Results from the toy galaxies considered here suggest that the (unpenalized) maximum-likelihood method nevertheless does yield reliable BH masses, but with overly pessimistic error estimates.

I confirm VME04's result that a wide range of BH masses can yield perfect fits to finite-resolution, noiseless observations. Contrary to their somewhat speculative arguments, however, I show that one does not expect to find flat-bottomed χ^2 distributions in practice, unless one is blessed with very high signal-to-noise observations (figure 3) and fits only the low-order shapes of the VPs.

Although the maximum-likelihood method yields reliable BH masses, it is flawed because it considers only one DF for each BH mass. The remedy is to consider all possible DFs for each potential, weighting each one by a suitably chosen prior. This significantly improves the constraints on the BH mass, since the closer a trial potential comes to the true potential, the greater the number of non-negative DFs that are consistent with the observations.

6.1 Open questions and future work

6.1.1 Choice of prior

An open question is to what extent these results depend on the choice of prior weights (equ. 26), and more generally on the use of the prior (23), which is just one of many possible infinitely divisible distributions. A very general argument (Kingman 1993) shows that drawing random realizations from most ID priors will yield spiky, uncorrelated distributions. This is just what one expects if dealing with galaxies at the level of individual stars, but the present models are far from this level of detail and one might plausibly expect some degree of correlation among neighbouring cells in phase space. Making this idea quantitative is difficult, however.

6.1.2 Computational scheme

It would be straightforward in principle to apply the ideas presented here to axisymmetric or triaxial galaxy models. One could simply adopt the prior (23), using the scheme described by Thomas et al. (2004) to calculate the volumes used to assign the prior weights μ . In practice, however, calculating the marginalized likelihood $p(D|\psi)$ will probably be very difficult. The DFs of axisymmetric galaxies are three-integral, which means that, in order to ensure a fine enough discretization, one has to use many more DF components than for two-integral spherical models, with the Markov Chain Monte Carlo procedure used in section 5.2 taking correspondingly more iterations to converge. On the other hand, it is very likely that there are much more efficient methods than the combination of Gibbs sampling and thermodynamic integration used here.

6.1.3 More immediate problems

Before applying this method to real galaxies though, it is probably worth addressing the following more tractable problems first:

(i) VPs are extracted from spectra, which suffer from poorly understood systematic errors (Houghton et al. 2006).

(ii) For real observations, neither individual VP velocity bins nor (surprisingly) Gauss-Hermite coefficients are independent (Houghton et al. 2006).

(iii) Most models of axisymmetric galaxies make an ad hoc assumption about the galaxy's three-dimensional light distribution $j(R, z)$, despite the fact that there are many $j(R, z)$ consistent with a given surface brightness distribution (e.g., Kochanek & Rybicki 1996). Neglect of this degeneracy can lead to incorrect inferences about the galaxy's orbit structure (Magorrian 1999) which are likely to affect BH mass estimates.

(iv) The widely used $\Delta\chi^2$ criteria for obtaining uncertainties on BH masses are based on the assumption that $\chi^2(M_\bullet, \Upsilon)$ is close to quadratic, which does not necessarily hold in practice.

ACKNOWLEDGMENTS

I thank James Binney, Karl Gebhardt, Andrew Jaffe, Douglas Richstone, Prasenjit Saha and Scott Tremaine for helpful discussions, the anonymous referee and the participants of the 2006 Lorentz Center workshop on Galactic Nuclei for comments that greatly improved the presentation of the results contained here, and the Royal Society for financial support.

REFERENCES

- Binney J., Tremaine S., 1987, *Galactic Dynamics*. Princeton University Press.
- Cappellari M., Verolme E. K., van der Marel R. P., Kleijn G. A. V., Illingworth G. D., Franx M., Carollo C. M., de Zeeuw P. T., 2002, *ApJ*, 578, 787
- Cretton N., Emsellem E., 2004, *MNRAS*, 347, L31
- Cuddeford P., 1991, *MNRAS*, 253, 414
- Dehnen W., 1993, *MNRAS*, 265, 250
- Dejonghe H., 1989, *ApJ*, 343, 113
- Dejonghe H., Merritt D., 1992, *ApJ*, 391, 531
- Feller W., 1971, *An introduction to probability theory and its applications*, vol 2., 2nd ed., Wiley.
- Gebhardt K., et al., 2003, *ApJ*, 583, 92
- Gerhard O. E., 1993, *MNRAS*, 265, 213
- Gull S. F., Daniell G. J., 1978, *Nature*, 272, 686
- Houghton R. C. W., Magorrian J., Sarzi M., Thatte N., Davies R. L., Krajnović D., 2006, *MNRAS*, 367, 2
- Kingman J. F. C., 1993, *Poisson Processes*. Oxford University Press.
- Kochanek C. S., Rybicki G. B., 1996, *MNRAS*, 280, 1257
- Lawson, C. L., & Hanson, R. J. 1974, *Solving Least Squares Problems* (Englewood Cliffs, New Jersey: Prentice-Hall)
- Magorrian J., 1999, *MNRAS*, 302, 530
- Magorrian J., Tremaine S., 1999, *MNRAS*, 309, 447
- Merritt D., 1993, *ApJ*, 413, 79

- Neal R. M., 1993, Technical Report CRG-TR-93-1, Department of Computer Science, University of Toronto
- Press W. H., Teukolsky S. A., Vetterling W. T., Flannery B. P., 1992, Numerical Recipes in C
- Richstone D.O., Tremaine S., 1988, ApJ, 327, 82
- Saglia R. P., Kronawitter A., Gerhard O., Bender R., 2000, AJ, 119, 153
- Schwarzschild M., 1979, ApJ, 232, 236
- Shu F. H., 1978, ApJ, 225, 83
- Silge J. D., Gebhardt K., Bergmann M., Richstone D., 2005, AJ, 130, 406
- Skilling J., 1998, "Massive Inference and Maximum Entropy", in Maximum Entropy and Bayesian Methods, G.Erickson, J.T.Rychert & C.Ray.Smith (eds) Kluwer Academic Publishers, Dordrecht, p. 14
- Thomas J., Saglia R. P., Bender R., Thomas D., Gebhardt K., Magorrian J., Richstone D., 2004, MNRAS, 353, 391
- Tremaine S., Richstone D. O., Byun Y., Dressler A., Faber S. M., Grillmair C., Kormendy J., Lauer T. R., 1994, AJ, 107, 634
- Valluri M., Merritt D., Emsellem E., 2004, ApJ, 602, 66 (VME04)
- van der Marel R. P., Franx M., 1993, ApJ, 407, 525
- van der Marel R. P., Cretton N., de Zeeuw P. T., Rix H.-W., 1998, ApJ, 493, 613
- van der Marel R. P., Magorrian J., Carlberg R. G., Yee H. K. C., Ellingson E., 2000, AJ, 119, 2038

APPENDIX A: OBSERVABLES OF DF COMPONENTS

I use a rectangular (x, y, z) co-ordinate system with origin O at the galaxy centre and whose Oz axis is parallel to lines of sight. Points on the plane of the sky are then labelled by the co-ordinates (x, y) . Of course, real observations do not have perfect spatial resolution. Instead, any function $f(x, y)$ defined on the plane of the sky is measured convolved with a two-dimensional point-spread function $\text{psf}(\Delta x, \Delta y)$:

$$f_{\text{meas}}(x, y) = \int \int \text{psf}(x - x', y - y') f(x', y') dx' dy'. \quad (\text{A1})$$

Since we assume that the galaxy is spherical, then $f(x, y) = f(R)$, where $R = \sqrt{x^2 + y^2}$ is the usual cylindrical polar radius, and the psf-convolved value of f at radius R ,

$$f_{\text{meas}}(R) = \int p(R, R') f(R') R' dR', \quad (\text{A2})$$

where

$$p(R, R') \equiv \int \text{psf}(R - R' \cos \phi', R' \sin \phi') d\phi' \quad (\text{A3})$$

is the azimuthally integrated contribution of light from radii R' to measurements at radius R . For example, in section 2 the toy galaxies are "observed" through annuli that admit light between some radii R_1 and R_2 . For this situation

$$p(R, R') = \frac{2}{|R_2^2 - R_1^2|} \times \begin{cases} 1 & \text{if } R_1 < R < R_2, \\ 0 & \text{otherwise.} \end{cases} \quad (\text{A4})$$

A more realistic psf is a Gaussian with some dispersion σ_* , for which

$$p(R, R') = \frac{1}{\sigma_*^2} \exp\left[-\frac{R^2 + R'^2}{2\sigma_*^2}\right] I_0\left(\frac{RR'}{\sigma_*^2}\right), \quad (\text{A5})$$

where I_0 is a Bessel function. Both these examples are symmetric, but we note that we can use (A2) and (A3) to convolve any spherically symmetric function $f(R)$ with a psf of arbitrary shape.

Now consider a single DF component (7) of energy \mathcal{E} and angular momentum J per unit mass in potential $\psi(r)$. Written explicitly as a function of (\mathbf{x}, \mathbf{v}) ,

$$f(\mathbf{x}, \mathbf{v}) = \delta\left[\psi - \frac{1}{2}(v_r^2 + v_\theta^2 + v_\phi^2) - \mathcal{E}\right] \delta[r^2(v_\theta^2 + v_\phi^2) - J^2]. \quad (\text{A6})$$

The individual orbits making up the DF component have peri- and apo-centre radii r_\pm given by the roots of the equation $V_r(r) = 0$, where

$$V_r^2(r) \equiv 2[\psi(r) - \mathcal{E}] - \frac{L^2}{r^2}, \quad (\text{A7})$$

and I have omitted the obvious dependence of the result on \mathcal{E} , J and ψ . The velocity moments of the component (A6),

$$\begin{aligned} [v_r^{2i} v_\theta^{2j} v_\phi^{2k}](r) &\equiv \int d^3\mathbf{v} v_r^{2i} v_\theta^{2j} v_\phi^{2k} f \\ &= 2B \left(i + \frac{1}{2}, j + \frac{1}{2}\right) \\ &\quad \times \begin{cases} \frac{V_r^{2i-1} J^{2(j+k)}}{r^{2(j+k+1)}} & \text{if } r_- < r < r_+, \\ 0 & \text{otherwise.} \end{cases} \end{aligned} \quad (\text{A8})$$

Taking $i = j = k = 0$ yields the luminosity density $j(r) = 2\pi/r^2 V_r$, which has integrable singularities at both $r = r_-$ and $r = r_+$. Integrating $j(r)$ over radius, the total luminosity of the component (A6) is given by

$$L = 8\pi^2 \int_{r_-}^{r_+} \frac{dr}{V_r}, \quad (\text{A9})$$

which is just the usual density-of-states factor.

Substituting $j(r)$ into equation (A2), the psf-convolved surface brightness distribution

$$\begin{aligned} I(R) &= 4\pi \int_0^\infty dR' p(R, R') R' \int_{-\infty}^\infty \frac{dz'}{(R'^2 + z'^2) V_r(R', z')} \\ &= 4\pi \int_{r_-}^{r_+} \frac{dr}{r^2 V_r} \int_0^{2\pi} p(R, r \sin \theta) \sin \theta d\theta. \end{aligned} \quad (\text{A10})$$

I evaluate this integral numerically by substituting $r = r_- + (r_+ - r_-) \sin^2 u$ and applying Simpson's rule with intervals $\Delta u = \pi/200$ and $\Delta \theta = \pi/50$. A simple test of this calculation is to compare the integrated surface brightness $2\pi \int RI(R) dR$ against the density-of-states factor (A9). I find that the two typically agree to around one part in 10^4 .

The calculation of velocity profiles is a little more involved. A star at position (R, z) with velocity (v_r, v_θ, v_ϕ) has projected line-of-sight velocity

$$v_p = \frac{1}{r} [zv_r + Rv_\theta]. \quad (\text{A11})$$

The luminosity density of stars located at a position (R, z)

having projected velocities in the range $v_1 < v_p < v_2$ is

$$\begin{aligned} j(R, z; v_1, v_2) &= \int_{v_1}^{v_2} dv_p \int f(\mathbf{x}, \mathbf{v}) \delta \left[\frac{1}{r} (zv_r + Rv_\theta) - v_p \right] d^3\mathbf{v} \\ &= \sum_{\pm} \int \frac{dv_p}{Rr|V_r V_{\phi\pm}|}, \end{aligned} \quad (\text{A12})$$

where the range of integration includes only those $v_p \in [v_1, v_2]$ for which

$$V_{\phi\pm}^2(R, z; v_p) \equiv \frac{J^2}{r^2} - \frac{(rv_p \pm zV_r)^2}{R^2} \quad (\text{A13})$$

is non-negative, and the \sum_{\pm} takes care of both possibilities for the sign of v_r . Integrating along the line of sight and using (A2), the (unnormalized) psf-convolved contribution of the DF component (A6) to a VP bin that extends from $v_p = v_1$ to v_2 is

$$\begin{aligned} \mathbb{L}(R; v_1, v_2) &= 2 \int_{r_-}^{r_+} r dr \times \\ &\int_0^{2\pi} p(R, r \sin \theta) j(R, r \cos \theta; v_1, v_2) d\theta. \end{aligned} \quad (\text{A14})$$

The integral (A12) for $j(R, r \cos \theta; v_1, v_2)$ can be carried out by hand, but finding efficiently the regions where it is nonzero is far from easy. So, to evaluate the double integral (A14) I simply adopt the scheme I use to calculate $I(R)$ and substitute $r = r_- + (r_+ - r_-) \sin^2 u$: the integration over v_p already takes care of the worst effects of the singularities in the integrand of (A12). To test this approach, I compare the integrated VP histogram, $\sum_i \mathbb{L}(R; i\Delta v, (i+1)\Delta v)$ for some choice of Δv , against $I(R)$. For my standard integration parameters, the typical RMS fractional difference between these two quantities is about 10^{-6} . This merely indicates that very little light “leaks” from the models, not that its VPs are calculated to that accuracy. Comparing VPs calculated with different stepsizes, I estimate that this standard integration scheme yields VPs with an RMS fractional error of a few parts in 10^4 .

To obtain the contribution each DF component makes to the modified moments $Ih_i(R)$, I calculate the component’s VP histogram $\mathbb{L}(R; v_i, v_{i+1})$ for 20 bins from $v_0 = 0$ to $v_{24} = 5\sigma$, where σ is the velocity dispersion used in the Gauss–Hermite expansion, and use this histogram in equation (4).

APPENDIX B: PRIORS

The following derivation of the prior (23) follows Skilling (1998). Imagine a monkey (Gull & Daniell 1978) with a bag of N identical stars each of luminosity L_* . He sits outside a big box containing phase space (strictly, integral space), takes each star in turn and throws it into the box. The probability of each star landing in a small volume $d^3\mathbf{x}d^3\mathbf{v}$ around the point (\mathbf{x}, \mathbf{v}) is $\alpha(\mathbf{x}, \mathbf{v})d^3\mathbf{x}d^3\mathbf{v}$. If we take a small cell of volume δV , the probability that r of the N stars land inside the cell is

$$p(r|N, \alpha\delta V) = \binom{N}{r} (\mu\delta V)^r (1 - \alpha\delta V)^{N-r}. \quad (\text{B1})$$

Now shrink the cell volume $\delta V \rightarrow 0$ and increase the number of stars $N \rightarrow \infty$ keeping the product $N\delta V$ constant.

Equation (B1) becomes

$$p(r|\alpha) = \frac{\alpha^r}{r!} e^{-\mu}, \quad (\text{B2})$$

describing a Poisson process with mean $\mu \equiv N\alpha\delta V$. Therefore, the probability of having luminosity L_i in a cell of phase-space volume V_i is given by

$$p(L_i|\mu_i) = e^{-\mu_i} \sum_{r=0}^{\infty} \frac{\mu_i^r}{r!} \delta(L_i - rL_*), \quad (\text{B3})$$

with $\mu_i \equiv N \int_{V_i} \alpha d^3\mathbf{x}d^3\mathbf{v} \simeq N\alpha_i V_i$. For a partition of phase space into n cells, the probability of the configuration (L_1, \dots, L_n) is given by a product of factors like (B3), which obviously satisfies the criterion (17) for infinite divisibility. Apart from uninteresting scale factors, this prior is identical to equation (20) of Shu (1978). In the limit $\mu_i \gg 1$ it takes on the entropy-like form $e^{-\mu} \exp[-(L/L_*)(1 + \ln(L/\alpha L_*))]$.

The prior (B3) has the disadvantage of requiring a discretization of the light into individual stars, with the result that L is very strongly peaked at 0 whenever $\mu \ll 1$. For an alternative, suppose that we place the monkey inside the box representing phase space and liquify his bag of stars so that the contents dribble out at a constant rate. Encumbered by his heavy bag of stellar light, the monkey sits at one point $(\mathbf{x}_i, \mathbf{v}_i)$ dribbling starlight unless disturbed. Every so often, however, we squeeze his tail and he jumps to a new position $(\mathbf{x}_{i+1}, \mathbf{v}_{i+1})$ with probability density $\alpha(\mathbf{x}_{i+1}, \mathbf{v}_{i+1})$. Let the tail squeezes be a Poisson process with rate λ , so that the distribution of time intervals between consecutive squeezes is $p(t) = \lambda e^{-\lambda t}$. More generally, the distribution of times between the i^{th} and $(i+r)^{\text{th}}$ squeezes follows a gamma distribution. Then, if the monkey lands r times in a cell of volume δV , the total length of time he spends in that cell has probability density

$$p(t|r) = \begin{cases} \lambda \delta(\lambda t), & r = 0; \\ \lambda e^{-\lambda t} (\lambda t)^{r-1} / (r-1)!, & r > 0. \end{cases} \quad (\text{B4})$$

In the limit of many tail squeezes, the probability that he lands r times in a cell of volume δV is again given by (B2). Summing over r , the probability distribution for the length of time he spends in the cell is

$$\begin{aligned} p(t|\mu) &= \sum_{r=0}^{\infty} p(t|r) p(r|\mu) \\ &= \lambda e^{-\mu} \left[\delta(\lambda t) + e^{-\lambda t} \sqrt{\mu/\lambda t} I_1(2\sqrt{\lambda t \mu}) \right], \end{aligned} \quad (\text{B5})$$

with the Bessel function I_1 coming in through the identity

$$\sum_{r=0}^{\infty} \frac{x^r}{r!(r+1)!} = \frac{1}{\sqrt{x}} I_1(2\sqrt{x}). \quad (\text{B6})$$

Equation (B5) is the ID prior (23) with $F = \lambda t$.